Inorganic Chemistry Communications 160 (2024) 111866

Contents lists available at ScienceDirect

Inorganic Chemistry Communications

journal homepage: www.elsevier.com/locate/inoche

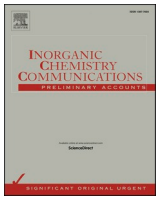

Short communication

Facile synthesis of carbon dots by the hydrothermal carbonization of avocado peels and evaluation of the photocatalytic property

Hela Ferjani [a], Sahar Abdalla [a], Opeyemi A. Oyewo [b], Damian C. Onwudiwe [c,d,*]

[a] Chemistry Department, College of Science, Imam Mohammad Ibn Saud Islamic University (IMSIU), Riyadh 11623, Saudi Arabia
[b] Department of Chemical Engineering, College of Science, Engineering and Technology, University of South Africa (UNISA), c/o Christian de wet &Pioneer Avenue, Florida Campus, 1710 Johannesburg, South Africa
[c] Department of Chemistry, School of Physical and Chemical Science, Faculty of Natural and Agricultural Sciences, Mafikeng Campus, North-West University, Private Bag X2046, Mmabatho 2735, South Africa
[d] Material Science Innovation and Modelling (MaSIM) Research Focus Area, Faculty of Natural and Agricultural Sciences, Mafikeng Campus, North-West University, Private Bag X2046, Mmabatho 2735, RSA, South Africa

ARTICLE INFO

Keywords:
Carbon quantum dots, biomass
Photodegradation
Dyes
Methyl orange

ABSTRACT

The preparation of carbon quantum dots (CQDs) from agricultural waste sources stands out as a significant type of biomass-based nanomaterials. This is primarily because of their minute size, exceptional water solubility, lack of toxicity, and impressive stability. Here, carbon quantum dots (CQDs) were successfully prepared by a one-step hydrothermal method using the waste from Avocado peels and only water as solvent. Physicochemical properties of the CQDs were characterized by UV–vis, PL, FTIR, XRD, SEM, TEM, and HRTEM. The diameter of the CQDs was found to satisfy the quantum size effect and this was also supported by the reduced graphitization. The CQDs were used for the removal of methyl orange (MO), a common anionic dye, from an aqueous solution. The effectiveness of MO removal was directly related to the pH and the amount of the nanomaterial used. Under optimal experimental conditions, with a 7.5 mg catalyst dose, a 120-minute reaction time, and a pH of 10, the maximum degradation of MO (78 %) was achieved.

1. Introduction

Quantum dots are semiconductor materials whose sizes in all three dimensions are confined to the nanoscale regime. Usually, these properties are dominated by materials composed mainly of metallic elements, such as CdTe, CdS, ZnSe, PbSe, and PbS quantum dots [1–5]. Despite their wide applications, informed by their interesting size-dependent properties, these types of metal-based QDs are associated with disadvantages such as high toxicity, expensive nature, inconvenience with handling, and environmental unfriendliness [6].

Carbon quantum dots (CQDs) are regarded as 0-dimensional carbon-based nanomaterials, comprised more of carbon whose sizes are between 2 and 5 nm. They can either be crystalline or amorphous structures, with sp^2 and sp^3 hybridized carbon atoms [7,8]. Since they were first discovered in 2004, they have attracted wide research attention and many intriguing studies due to their fascinating properties, including ease of functionalization, high chemical stability, exceptional solubility, environmental friendliness, and high photoluminescence compared to the one-dimensional carbon nanomaterials such as carbon nanotubes [9]. The exceptional qualities of these materials have rendered them remarkable in numerous applications including medical diagnosis, photodegradation, fluorescent sensors, optoelectronic devices, white light emitting diodes (WLED), cellular labeling, and biosensing. This is due to their intriguing features such as multicolor optical properties, high solubility in water, excellent chemical stability, non-toxic nature, and biocompatibility [8].

Although small organic molecules including urea, glucose, and organic acids could serve as precursors to carbon dots [10], the CQDs development from waste and cheap biomass offers a huge advantage. Natural organic products, cellulose, and carbohydrate are the main constituent of biomass [11]. Therefore, it is important to continue the development of facile, cost-effective, and environmentally favourable methods based on affordable precursor materials. The current study is based on the use of natural biomass as a precursor to synthesize CQDs

* Corresponding author at: Department of Chemistry, School of Physical and Chemical Science, Faculty of Natural and Agricultural Sciences, Mafikeng Campus, North-West University, Private Bag X2046, Mmabatho 2735, South Africa.
E-mail address: damian.onwudiwe@nwu.ac.za (D.C. Onwudiwe).

https://doi.org/10.1016/j.inoche.2023.111866
Received 19 October 2023; Received in revised form 1 December 2023; Accepted 9 December 2023
Available online 10 December 2023

with stable physicochemical properties. Natural biomaterials are a better choice over materials of inorganic, organic, or synthetic alternatives. Research attention has been drawn to the CQDs preparation using biomass precursors [12–14]. On the other hand, traditional chemical and physical approaches are less acceptable compared to the green method of synthesis. The hydrothermal technology, which utilises natural raw materials has gained much attention recently due to its environmental friendliness and other highlighted benefits. Other studies have focused on the doping of the CQDs using the minerals that are present in natural biomaterials, which facilitate the insertion of heteroatoms as dopants without utilising any dopant precursors [15].

The increase in water contamination due to organic pollutants has become a pressing global concern, posing significant threats to human health, ecological stability, and biodiversity. Dyes, in particular, have seen a sharp rise in water bodies. Human activities such as the discharge of untreated effluents from industrial wastewater are the primary contributors to the infiltration of dyes into aquatic environments. The textile industries stand as a significant contributor to global dye pollution, consuming substantial amounts of fuel. Textile dyes, when released into water bodies, drastically impair visual clarity, elevate biochemical and chemical oxygen demands, disrupt natural photosynthesis, hinder the growth of plants, and infiltrate the food chain. Azo dyes constitute 70% of all commercial dyes utilized in the textile industries across the world [16] and Methyl orange (MO) is a common example. It is an anionic dye whose widespread use has led to significant ecological issues owing to its harmful effects and possible accumulation in living organisms. Its health effects are due to its toxicity, carcinogenicity, mutagenicity, and teratogenicity [17].

Herein, we prepared CQDs from the hydrothermal treatment of avocado peel waste and assessed its potential for the removal of MO under UV light. Characterization techniques including UV–vis, PL, FTIR, XRD, SEM, TEM, and HRTEM were used to establish the optical, structure, and morphology of the nanomaterial. The experimental parameters such as the effect of solution pH, catalyst dosage, and dye concentration were used to evaluate the performance of the CQDs in the photodegradation of the MO.

2. Experimental details

2.1. Chemicals, Materials, and methods

Avocado fruit was bought from a Fruit Supermarket store in the Kingdom of Saudi Arabia and properly identified. Teflon-coated stainless-steel autoclave was used for carbonization. All other chemicals such as methyl orange (MO) and sodium hydroxide (for pH adjustment) were purchased from Sigma-Aldrich. These reagents were used without further purification. Distilled water was used as solvent throughout the experiment.

2.2. Characterization of carbon quantum dots

The diffraction patterns in the range of $2\theta = 20 - 80^{\circ}$ was measured using a Bruker D8 Advanced, which is equipped with a proportional counter that uses Cu Kα radiation (k = 1.5405 A, nickel filter). TEM analysis was carried out using TECNAI G2 (ACI) transmission electron microscopy with an accelerating voltage of 200 kV and it was undertaken to validate the morphology and size of the nanoparticles. Surface morphologies were assessed with a scanning electron microscope using a LYRA 3, TESCAN at 15–20 kV. UV–vis measurement was conducted on a Cary 300 UV–vis spectrophotometer (Agilent technologies). Photoluminescence studies were on a Perkin Elmer LS 45 fluorescence spectrophotometer. The assessment of the functional group was by FTIR spectroscopy measured in the 4000——400 cm^{-1} range using a Cary 670 FTIR spectrometer (Agilent Technologies).

2.3. Development of carbon quantum dots derived from avocado peels

Briefly, the avocado peels were cut into pieces and ground with distilled water to form a paste. This was transferred into a Teflon-lined stainless steel mini-autoclave, tightly sealed, and was placed in a furnace where the sample was heated at 180 °C for 24 h. Thereafter, the obtained brown product was filtered using a 0.22 μm mixed cellulose ester membrane to screen out larger particles. The supernatant was freeze-dried for 48 h and the yield of the carbon dots was calculated from the initial weight of the starting material (4 g of dry avocado peels) and the final weight of the carbon dots (0. 592 g) was 14.81%. The dark brown carbon quantum dots were stored in the fridge at 4 °C for characterization.

2.4. Photocatalytic experiments

The investigation of the catalytic activity of the CQDs was conducted using a photocatalytic reactor equipped with a 20 W lamp as the light source. Initially, about 0.25 mg of the carbon dots were added to a 100 mL solution of MO dyes (1.2×10^{-5} M). The mixture was kept in the darkroom and stirred for about 30 min to achieve an absorption and desorption equilibrium. Thereafter, the solution was irradiated with light and their absorbance was monitored using a UV–vis spectrophotometer in a range of 250 – 750 nm. The percentage degradation of the MO was computed from the following Eq. (1) [18].

$$\%\,Degradation(\%) = \frac{A_0 - A_t}{A_0} \times 100 \quad (1)$$

3. Results and discussion

3.1. XRD studies

The diffraction pattern of the synthesized carbon QDs presented in Fig. 1 shows the peaks at $2\theta = 24.5^{\circ}$ and 42.8°, which correspond to the (0 0 2) and (1 0 0) planes respectively of carbonaceous materials [19]. The (0 0 2) plane is ascribed to the arrangement of disordered carbon atoms within the hexagonal graphite structure of carbon quantum dots, leading to the formation of a turbostratic structure through interlayer packing (JCPDS No. 26–1076) [20]. Hence, the carbon dots exhibit mainly carbon framework consisting of a graphitic, and this structure exhibits interlayer spacings of 0.38 nm and 0.21 nm, corresponding to the (0 0 2) and (1 0 0) diffraction, respectively. [21]. Compared to the d-spacing between the (0 0 2) planes of typical bulk graphite (~0.34 nm), this is larger and is attributed to the amorphous nature of the carbon structure. Hence, these two diffraction peaks are characteristic signature peaks of carbon that indicate nanostructures made up of mainly densely packed carbon and oxygen atoms [22].

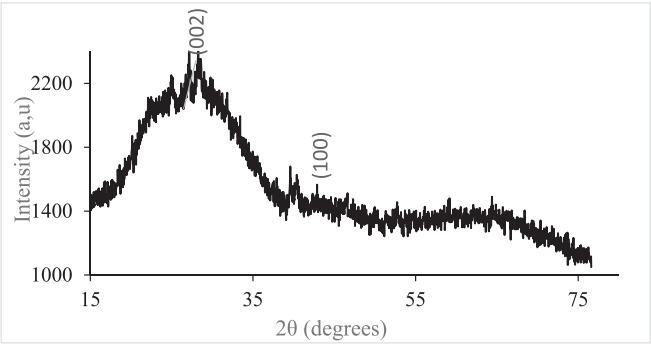

Fig. 1. XRD pattern of carbon QDs obtained from hydrothermal carbonization of avocado peels.

3.2. Morphological studies

The microscopic properties of the carbon dots were determined using TEM analysis and are shown in Fig. 2. The results (Fig. 2a and b) indicate that the particles are spherical, homogeneously monodispersed, and with no form of aggregation. The estimated particle size is about 2.9 nm, and the size distribution histogram (Fig. 2c) presents a narrow size distribution of the carbon dots, which also attests to the size of the CQDs. The HRTEM image (Fig. 2d) showed distinct lattice fringes with a lattice spacing of 2.1 nm corresponding to the (1 0 0) of the lattice planes of CQDs and implies high crystallinity of the synthesized quantum dots. The QDs showed that the lattice spacing is approximately 0.23 nm and it is due to the (1 0 0) plane characteristic of graphene. Similar morphology of carbon dots has been reportedly obtained from green material [23].

The surface morphology of the CQDs was analysed using SEM technique, and Fig. 3 a and b present the SEM micrographs at lower and higher magnification respectively. As shown in both images, the SEM images reveal spherically shaped nanoparticles with distinct edges that corroborate the TEM results. The EDX analysis with spectrum displayed in Fig. 3c showed that carbon, oxygen, and nitrogen can be detected, and the elemental mapping micrographs depict that these elements are uniformly distributed. These correspond to the elemental composition shown in the EDX results and confirm the effectiveness of the hydrothermal carbonization method.

3.3. Fourier transform infrared studies

The carbon skeleton of CQDs is often draped with several functional groups due to the presence of different hybridizations [24], as displayed in the IR spectrum of the CQDs (Fig. 4). The strong peak around 1635 cm^{-1} could be attributed to the C = O stretch of a secondary amide. Typical of all amides, this peak often appears in the 1680 to 1630 cm^{-1} range and has a companion peak around 1540 cm^{-1}, which is identified here at 1534 cm^{-1}. This peak is described as the in-plane N–H bending vibration of the secondary amide and the range of its appearance is often from 1570 to 1515 cm^{-1}. [25,26]. The NH stretching vibrations intramolecularly bonded to the other molecules peak appear at 3278 cm^{-1}, and it is followed by the stretching vibrations of -C–H around 2924 cm^{-1} [27]. The peak at 1382 cm^{-1} corresponds to the C–N stretching vibrations of amide. It is important to highlight that the presence of these functional groups is critical because they determine certain properties exhibited by the quantum dots such as wettability and compatibility with other materials since they improve the interaction between the quantum dots and the substrate materials [28].

3.4. Optical studies

The UV–vis spectrum of the carbon quantum dots presented in Fig. 5a, reveals a typical absorption spectrum of synthesized CQDs. The main features are the absorption peaks around 285 nm, which could correspond to the π–π* transition derived from the carbon core [29], and a slight shoulder at 343 nm that corresponds to the n–π* transitions of the sp2 hybridized carbon [10]. The n – π* band is based on the trapping of the excited state energy on the surface of the CQDs [30]. This is consistent with similar reports involving the development of CQDs derived from biomass materials [31,32]. Fig. 5(b) shows the estimation of the bandgap energy value of the CQDs, from the Tauc-plot method. The band gap energy was found to be 3.4 eV, which is consistent with the previous reports indicating that CQDs have bandgap energy values within 1.5–3.5 eV range [33]. It is important to note that smaller size results in larger band gap values and this implies that a higher energy is needed to release electrons from the valence band of the nanomaterial to the conduction band [34,35]. The energy shift effect usually created by particle size is referred to as the quantum size effect.

The photophysical properties of carbon dots and the peak intensity are dependent on the excitation wavelength. Hence, the optical behavior of the carbon dots was further investigated using PL spectroscopy which displays the excitation-dependent fluorescence emission peaks [36]. Emission spectra were recorded in water at different excitation wavelengths (Fig. 6). The strongest fluorescence emission wavelength was at 404 nm using the excitation wavelength of 350 nm. Variation in the excitation wavelength from 350 to 500 nm resulted in a noticeable decrease in intensity. A definitive property of quantum confinement in carbon dots is observed in its size-dependent PL and this is exhibited as excitation-dependent photoluminescence properties. The PL spectra are commonly broad, extending from the visible to the near-infrared region in accordance with the wavelength at which it was excited [37]. This excitation dependence of the PL spectra of carbon dots has been reported to be majorly due to the size differences rather than the difference in the emissive trap sites on similarly sized particles [38]. The photoluminescence property of the brown-yellow carbon quantum dots was confirmed by the blue coloration under UV light. It is observed that with a further increase in λ_{ex} from 440 to 500 nm, the PL emission peaked at ~ 440 nm indicating a red shift from the 404 nm. The decrease in the

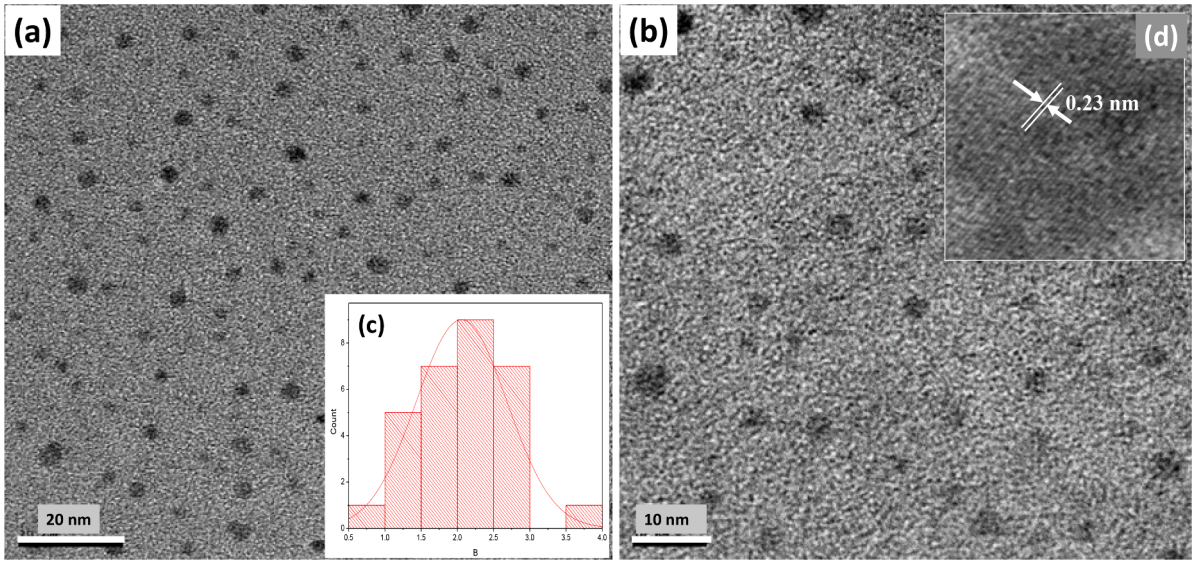

Fig. 2. TEM micrograph of carbon QD at (a) Low magnification, (b) high magnification, (c) Particle size distribution histogram, and the (d) High resolution TEM image.

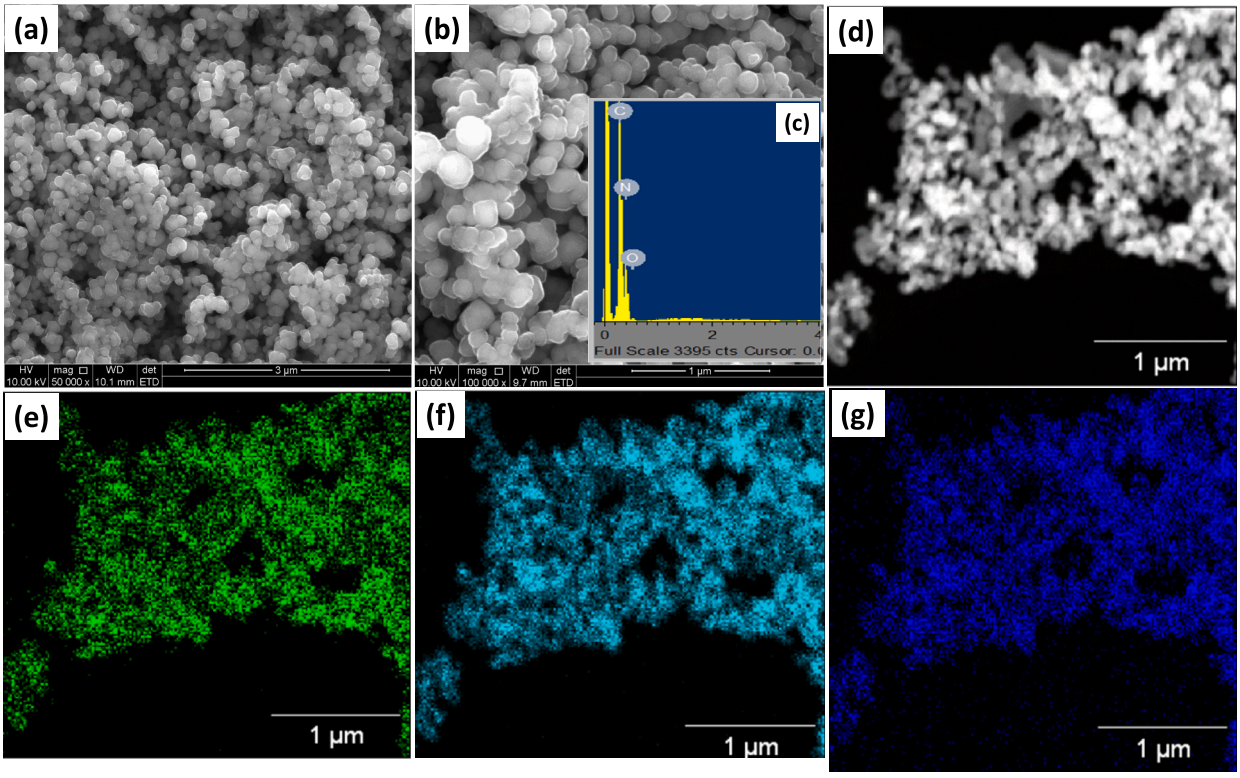

Fig. 3. SEM images of carbon QD at (a) lower and (b) higher magnification; (c) EDX spectrum (inset); (d) elemental mapping showing, (c) C, O, and (d) N of CQDs obtained from hydrothermal carbonization of avocado peels.

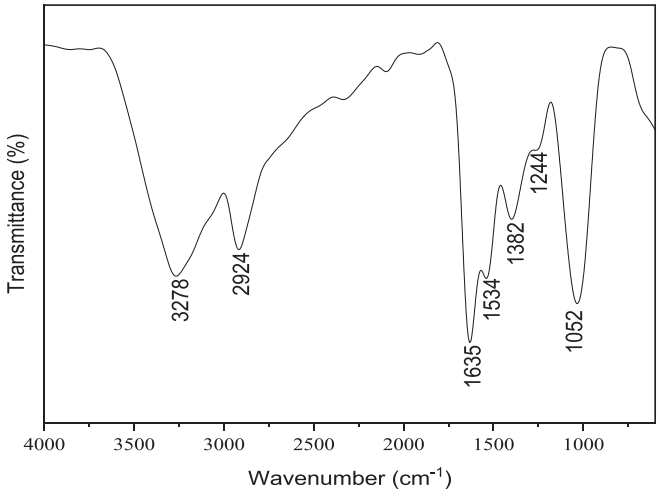

Fig. 4. FTIR spectrum of CQDs prepared from hydrothermal carbonization of Avocado peels waste.

peak intensity as well as the red shifting of the peaks are consistent with previous reports. The phenomena have been ascribed to the variation of the CQD's size, the occurrence of different trap states, and presence of different polyaromatic fluorophores that exist within the carbon skeleton [39,40]. In addition, larger particle sizes result to the delocalization of π-electron in the sp^2 domain leading to the redshift of the emission wavelength [41].

Quantum yield have been calculated using quinine sulphate (QS) in 0.1 M H_2SO_4 as a standard following an established procedure. It was calculated in water as a reference, the fluorescence intensity of quinine sulphate with the QY of 53 % in 0.1 mol L^{-1} H_2SO_4 (n = 1.33) at 350 nm excitation. An absorbance plot of the quinine sulphate and the carbon

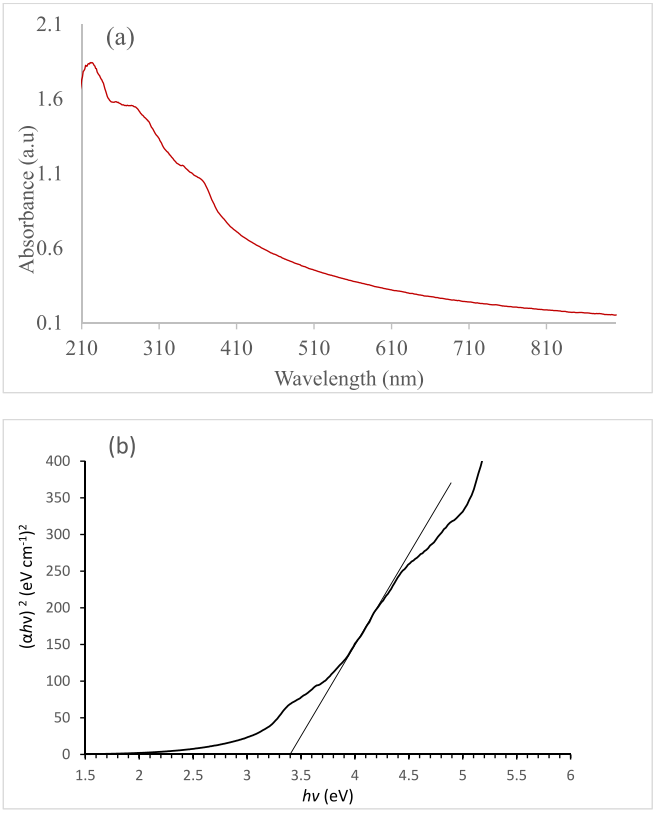

Fig. 5. UV–vis absorption spectrum of carbon QDs obtained from a hydrothermal process using avocado peel waste.

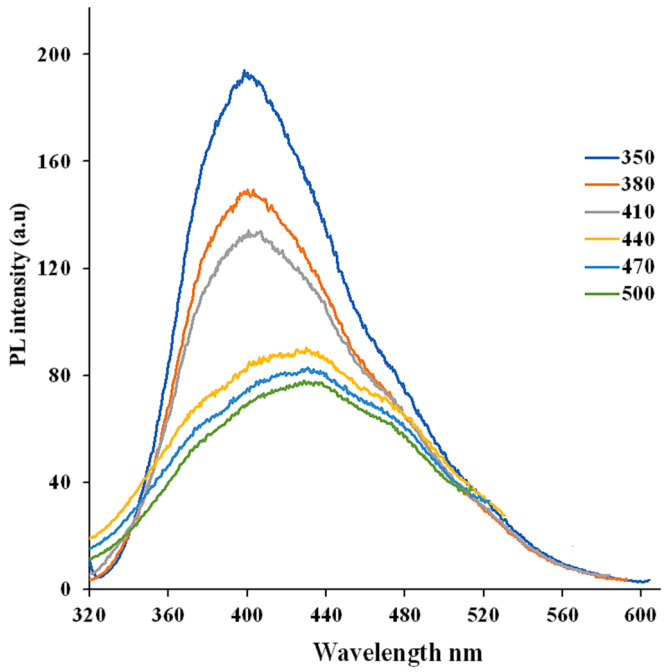

Fig. 6. Photoluminescence spectra of carbon quantum dots under excitation wavelength of (a) 350 (b) 380 (c) 410 (d) 440 (e) 470 (f) 500 nm.

dots was analyzed using the following equation (2) [42].

$$\Phi_u = \Phi_s(Y_u/Y_s)(A_s/A_u)(\eta_s/\eta_u)^2 \quad (2)$$

where: Φ denotes the QY, subscripts s and u signifies the values for the quinine sulphate (used as reference) and the carbon dots; Y represents emission peak integrated area, the absorbance at 350 nm is denoted by A, and η ($\eta_s = 1.369$, $\eta_u = 1.332$) represents the refractive index. Note: For this study, η_u/η_s was approximated to 1 [43,44].

3.5. Catalytic degradation of methyl orange using the CQDs

The functional groups on carbon QDs facilitate their photocatalytic activity for the photo-enhanced degradation of organic dyes. Upon the absorption of a photon, electrons which are in the HOMO (highest occupied molecular orbital) are excited to the LUMO (lowest unoccupied molecular orbital), thereby resulting in the generation of oxidative holes in the HOMO and the reduction of electrons in the LUMO. Variations in intensities could be observed due to the presence of specific groups like O or N atoms, the emergence of electronic fields that were not in the original band structure, and an increase in bending bands on the CQDs' surface. Additionally, the presence of NH, COOH, and OH groups increases the hole-electron pairs and enhances the photocatalytic activity [45,46].

The catalytic efficiency of the CQDs was assessed by studying the breakdown of methyl orange. The time-dependent degradation of methyl orange over a 120 min reaction is presented in Fig. 7a. The catalyst was able to achieve about 76% degradation of the MO dye within the 120 min studied time without any co-catalyst (Fig. 7b).

The kinetics of the degradation process was investigated and the pseudo-first order reaction kinetics obtained using equation (3) are presented in Fig. 7c and d.

$$lnC_o - lnC_t = kt \quad (3)$$

where, MO's initial and final concentrations are represented by C_o and C_t (mg/L) respectively, k is the reaction rate constant (min^{-1}), and t is the irradiation time (min).

The catalytic degradation of the MO was found to follow a pseudo-first-order reaction kinetics, which is in agreement with other previous

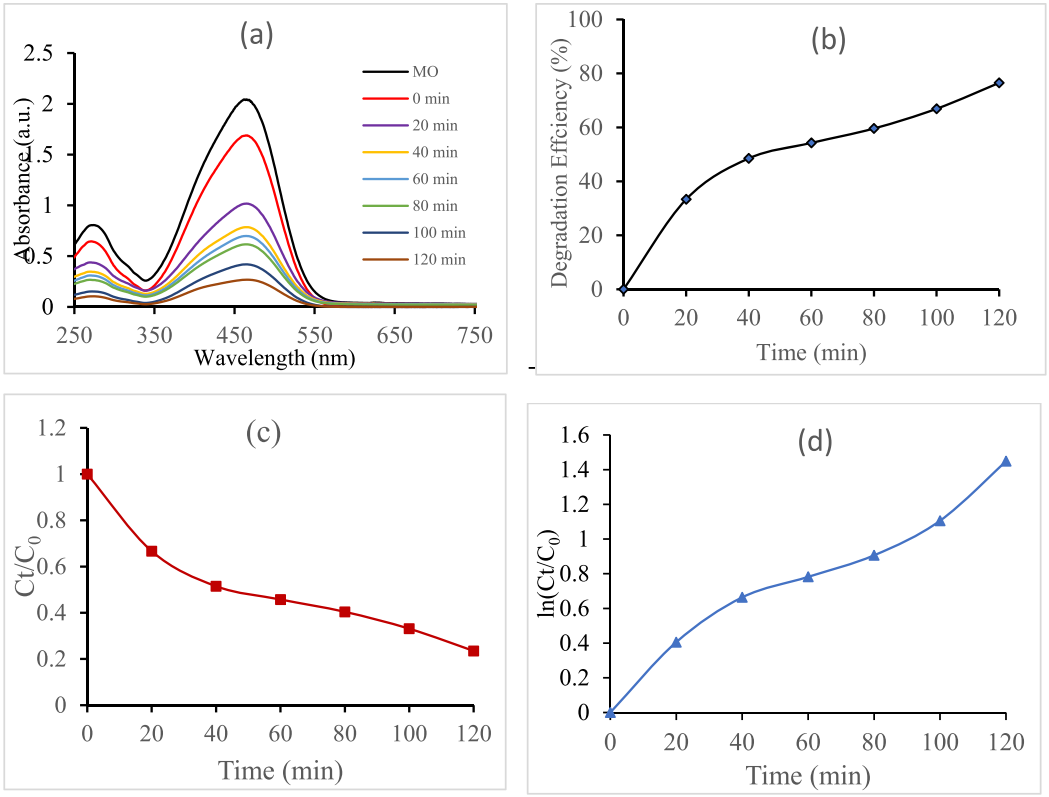

Fig. 7. Catalytic degradation of MO: (a) Absorption spectra showing the degradation of MO with time, (b) the degradation efficiency, (c) a plot of (C/C_0) vs. time, and (d) $\ln(C/C_0)$ vs. time reaction.

studies [47].The effect of different kinetic parameters, including the dye concentration, photocatalyst dosage, and solution pH on the degradation rate of the dye molecules.

3.5.1. Effect of dye concentration on the degradation efficiency

To investigate the impact of MO's initial concentration on the efficiency of the CQD, a study was conducted under UV light. In this study, the concentration of the CQDs (0.25 mg) was kept constant while the amount of the MO (1.2×10^{-5} M, 100 mL) was varied to double and triple concentrations. The MO solutions were exposed to the light for a 120 min time and the absorption was measured at specific intervals using an absorption spectrophotometer. The results presented in Fig. 8 show that more dye molecules were destroyed at lower concentration and the increased concentration of the dye molecules would imply that a longer reaction time would be required to achieve the same degradation rate recorded at lower dye concentration.

3.5.2. Effect of pH on the degradation efficiency

The solution pH affects the degradation process of MO molecules based on the charged functional groups that are present in the carbon dots. In the synthesized nanomaterial, the study of the effect of pH values on the rate of dye degradation was necessary. Therefore, a range of solution pH 4, 7, and 10 representing acidic, neutral, and basic were used while a fixed initial dye concentration (1.5×10^{-5} M) and catalyst dosage of 0.25 mg were maintained under the UV light irradiation. The dye solution was irradiated by the UV light for 120 min, while aliquots were taken at definite intervals and the adsorption was measured using an absorption spectrophotometer. The percentage MO degradation at the selected pH values was determined using Equation (1) and the results are presented in Fig. 9. The result shows an increase in the percentage degradation of MO with an increase in pH. The graph showed that the highest percentage degradation was achieved at pH 10, which showed an 84% efficiency, while pH 4 exhibited the lowest percentage degradation of the catalyst with a degradation efficiency of 68%. This indicates the significant effect that the solution pH has on the rate of degradation rate and confirms the relationship that exists between the MO solution pH and the photocatalyst's surface potential [48].

Previous studies have attributed the effect of pH on the degradation efficiency of dye molecules to the presence of hydroxyl radicals ($OH\bullet$) generated by the holes that are present in the valence band (h^{+}_{VB}) due to the excitation of electrons in the carbon QDs. Some hydroxyl radicals are also generated by the reaction of OH– ions and H_2O molecules as shown in Equations (4) and (5):

$$OH^{-} + h^{+}_{VB} \rightarrow OH^{\bullet} \quad (4)$$

$$H_2O + h^{+}_{VB} \rightarrow OH^{\bullet} + H^{+} \quad (5)$$

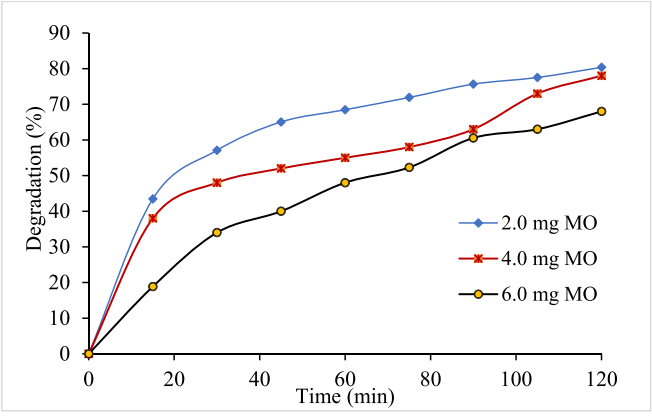

Fig. 8. The effects of MO dye concentration on the photodegradation activity of the carbon QDs.

Since $OH^{\bullet}$ are very strong oxidizing radicals, they can attack and destroy the azo group (N = N), which is responsible for the orange colour of the MO molecule and this is responsible for the removal of MO from the solution. Also, these radicals could target the aromatic structures present in the dye as well, although the degradation process occurs after the dye has been decolorized [49]. Furthermore, the influence of pH on the photocatalytic process may be attributed to the following factors: a) presence of comparatively high concentration of H^{+} ions in the reaction medium. The existence of these charged ions creates a competition between the H^{+} ions and dye molecules seeking adsorption sites on the surface of the quantum dots. In addition, the high mobility of the H^{+} ions compared to the dye molecules further accentuates their ability for fast binding to the negatively charged QDs. Hence, the number of vacant sites available on the surface of the QDs for the adsorption of the dye molecules is reduced. Furthermore, under low pH conditions, H^{+} ions form bonds with the azo group, thereby diminishing its electrophilic nature. b) pH levels impact both dye and photon adsorption [50,51]. In the environment of the basic solution, the functional groups acquire more negative charges, which proves to be a valuable factor in the transition of electrons during the MO degradation [48].

Studies conducted by Chaudhary et al., [52] reported the highest removal of dye molecules at neutral pH 7. This outcome was attributed to the reduction in the corresponding amount of H^{+} ions with increasing pH of the reaction medium, which resulted in the higher adsorption tendency of the MO molecules to the surface of the QDs.

3.5.3. Effect of the concentration of CQDs

To optimize the amount of applied CQDs, a constant dye concentration (1.2×10^{-5} M) was prepared at the optimal pH (10). This solution was mixed with different concentrations of the CQDs and the resulting mixture was irradiated with UV light for 120 min. This was followed with the measurement of absorption rate at specific time intervals using a spectrophotometer and Eqn 1 was used to calculate the percentage degradation of the dye in each solution. The result is presented in Fig. 10, which shows that an increase in the number of catalysts resulted to a decrease in the percentage degradation of the dye. This is because the enhancement in the amount of carbon QDs could increase its accumulation, which ultimately could reduce the percentage of dye degradation.

3.5.4. Reusability studies

The reusability studies of the carbon QDs were conducted by washing the photocatalyst thoroughly using distilled water and reusing it for the degradation of methyl orange for four consecutive cycles (Fig. 11). After the fourth cycle, the degradation of methyl orange decreased from 78 to 70% within 480 min, indicating good reusability.

4. Conclusion

Cost-effective and environmentally friendly CQDs were synthesized from naturally available avocado peels waste by hydrothermal route. The optical, structural, and morphology of the carbon quantum dots were characterized using techniques such as UV–vis, FTIR, XRD, SEM, TEM, and HR-TEM. Spherical and homogenously dispersed uniform morphology with a size of about 2.22 nm and maximum fluorescence at 404 nm were confirmed. The prepared CQDs were utilized for the degradation of MO dye and up to 78% dye removal efficiency was recorded. From these results, it is concluded that the Avocado peel-derived CQDs, if modified, could be highly promising for the degradation of dye from aqueous solution.

CRediT authorship contribution statement

Hela Ferjani: Investigation, Formal analysis, Writing-original draft. **Sahar Abdalla:** Methodology, Resources. **Opeyemi A. Oyewo:**

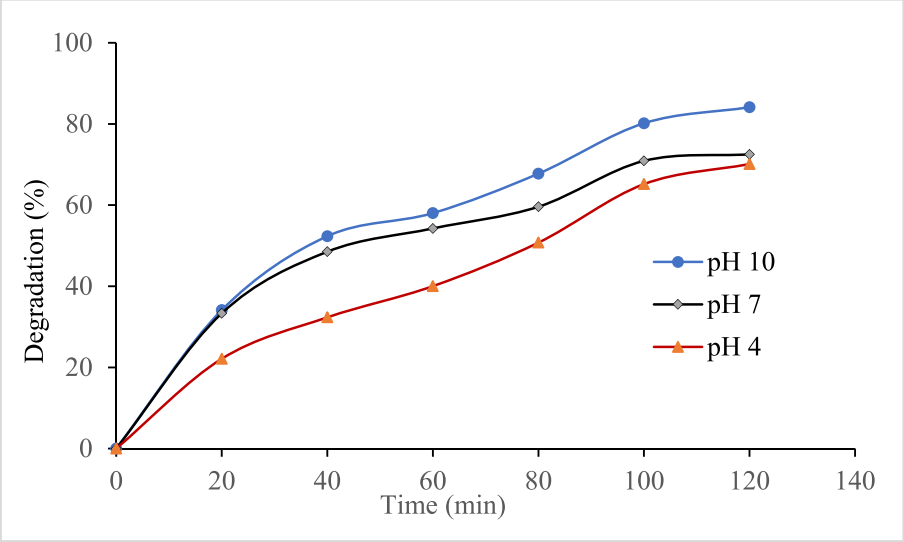

Fig. 9. The effects of solution pH on the photodegradation activity of the carbon QDs.

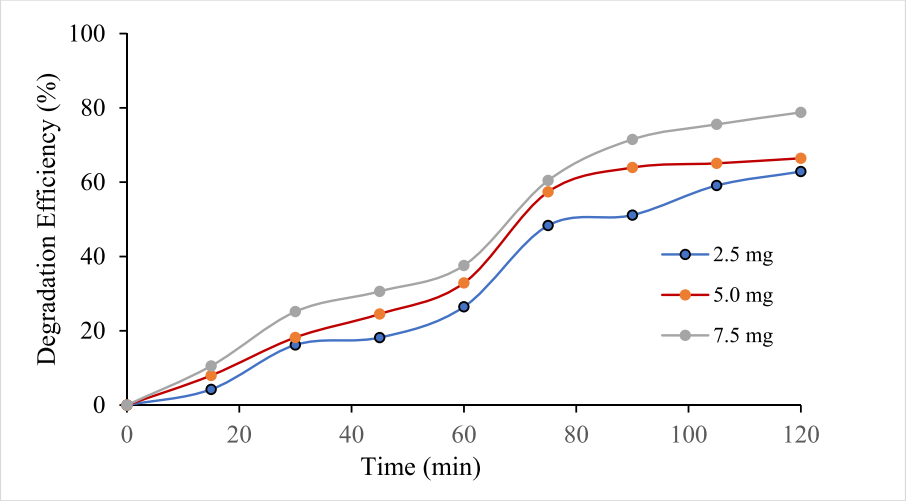

Fig. 10. The effects of the amount of carbon QDs on the photodegradation activity of the carbon QDs.

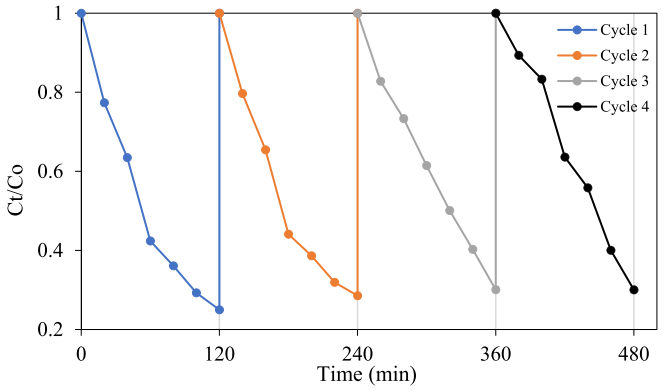

Fig. 11. Reusability results of the photocatalyst over four cycles for the photodegradation of methyl under visible-light irradiation.

Methodology, Writing-original draft. **Damian Onwudiwe:** Conceptualization, Writing-review & editing.

Declaration of competing interest

The authors declare that they have no known competing financial interests or personal relationships that could have appeared to influence the work reported in this paper.

Data availability

Data will be made available on request.

Acknowledgments

This work was supported and funded by the Deanship of Scientific Research at Imam Mohammad Ibn Saud Islamic University (IMSIU) (grant number IMSIU-RP23113).

References

[1] F.S. Riehle, K. Yu, Role of alcohol in the synthesis of CdS quantum dots, Chem. Mater. 32 (2020) 1430–1438.
[2] E. Pérez-Barrado, L.F. Marsal, M. Aguiló, Y. Cesteros, F. Díaz, J. Pallarès, F. Cucinotta, L. Marchese, M.C. Pujol, P. Salagre, Thiol-capped CdTe quantum dots hosted in saponites, RSC Adv. 6 (2016) 104793–104798.
[3] Z. Bai, L. Hao, Z. Huang, S. Qin, Z. Zhang, Enhancement effect of defect fluorescence of ZnSe quantum dots on a heterojuction of ZnSe quantum dots and gold nanoparticles, Method. Appl. Fluoresc. 5 (2017), 045001.
[4] M.S. Zaini, J. Ying Chyi Liew, S.A. Alang Ahmad, A.R. Mohmad, M.A. Kamarudin, Quantum confinement effect and photoenhancement of photoluminescence of PbS and PbS/MnS quantum dots, Appl. Sci. 10 (2020) 6282.
[5] V. Notot, W. Walravens, M. Berthe, N. Peric, A. Addad, X. Wallart, C. Delerue, Z. Hens, B. Grandidier, L. Biadala, Quantum dot acceptors in two-dimensional epitaxially fused PbSe quantum dot superlattices, ACS Nano 16 (2022) 3081–3091.
[6] Y. Zhao, L. Yu, Y. Deng, K. Peng, Y. Yu, X. Zeng, A multi-color carbon quantum dots based on the coordinated effect of quantum size and surface defects with green synthesis, Ceram. Int. 49 (2023) 16647–16651.
[7] Y. Zhao, Y. Zhang, X. Liu, H. Kong, Y. Wang, G. Qin, P. Cao, X. Song, X. Yan, Q. Wang, Novel carbon quantum dots from egg yolk oil and their haemostatic effects, Sci. Rep. 7 (2017) 4452.
[8] K. Kumar, A. Kumar, S. Devi, S. Tyagi, D. Kaur, Relevant photovoltaic effect in N-doped CQDs/MoS2 (0D/2D) quantum dimensional heterostructure, Ceram. Int. 48 (2022) 14107–14116.
[9] F. Mindivan, M. Göktaş, The green synthesis of carbon quantum dots (CQDs) and characterization of polycaprolactone (PCL/CQDs) films, Colloids Surf A Physicochem Eng Asp 677 (2023), 132446.
[10] A. Sharma, J. Das, Small molecules derived carbon dots: synthesis and applications in sensing, catalysis, imaging, and biomedicine, J. Nanobiotechnol. 17 (2019) 1–24.
[11] V. Manikandan, N.Y. Lee, Green synthesis of carbon quantum dots and their environmental applications, Environ. Res. 212 (2022), 113283.
[12] X. Wang, S. Gao, N. Xu, L. Xu, S. Chen, C. Mei, C. Xu, Facile synthesis of phosphorus-nitrogen doped carbon quantum dots from cyanobacteria for bioimaging, The, Can. J. Chem. Eng. 99 (2021) 1926–1939.
[13] K. Hagiwara, S. Horikoshi, N. Serpone, Luminescent monodispersed carbon quantum dots by a microwave solvothermal method toward bioimaging applications, J. Photochem. Photobiol. A Chem. 415 (2021), 113310.
[14] L.J. Desmond, A.N. Phan, P. Gentile, Critical overview on the green synthesis of carbon quantum dots and their application for cancer therapy, Environm. Sci. Nano 8 (2021) 848–862.
[15] V. Kansay, V.D. Sharma, G. Chandan, I. Sharma, A. Bhatia, S. Chakrabarti, M. K. Bera, Facile green synthesis and characterization of fluorescent nanoprobe based on Ca, K, N-doped carbon quantum dots derived from Aegle marmelos for bioimaging of human neuroblastoma cancer cells and living organisms, Dyes Pigm. 218 (2023), 111477.
[16] R. Krishnamoorthy, A. Roy Choudhury, P. Arul Jose, K. Suganya, M. Senthilkumar, J. Prabhakaran, N.O. Gopal, J. Choi, K. Kim, R. Anandham, Long-term exposure to azo dyes from textile wastewater causes the abundance of Saccharibacteria population, Appl. Sci. 11 (2021) 379.
[17] A. Grover, I. Mohiuddin, A.K. Malik, J.S. Aulakh, K. Vikrant, K.-H. Kim, R.J. Brown, Magnesium/aluminum layered double hydroxides intercalated with starch for effective adsorptive removal of anionic dyes, J. Hazard. Mater. 424 (2022), 127454.
[18] Z. Sabouri, M. Sabouri, M.S. Amiri, M. Khatami, M. Darroudi, Plant-based synthesis of cerium oxide nanoparticles using Rheum turkestanicum extract and evaluation of their cytotoxicity and photocatalytic properties, Mater. Technol. 37 (2022) 555–568.
[19] R. Atchudan, T.N.J.I. Edison, M.G. Sethuraman, Y.R. Lee, Efficient synthesis of highly fluorescent nitrogen-doped carbon dots for cell imaging using unripe fruit extract of Prunus mume, Appl. Surf. Sci. 384 (2016) 432–441.
[20] V. Kansay, V.D. Sharma, G. Chandan, I. Sharma, S. Chakrabarti, M. Bera, Sustainable synthesis of nitrogen-doped fluorescent carbon quantum dots derived from Cissus quadrangularis for biomarker applications, Mater. Chem. Phys. 296 (2023), 127237.
[21] R. Atchudan, T.N.J.I. Edison, M. Shanmugam, S. Perumal, T. Somanathan, Y. R. Lee, Sustainable synthesis of carbon quantum dots from banana peel waste using hydrothermal process for in vivo bioimaging, Physica E 126 (2021), 114417.
[22] A. Hao, X. Guo, Q. Wu, Y. Sun, C. Cong, W. Liu, Exploring the interactions between polyethyleneimine modified fluorescent carbon dots and bovine serum albumin by spectroscopic methods, J. Lumin. 170 (2016) 90–96.
[23] X. Zhao, S. Liao, L. Wang, Q. Liu, X. Chen, Facile green and one-pot synthesis of purple perilla derived carbon quantum dot as a fluorescent sensor for silver ion, Talanta 201 (2019) 1–8.
[24] G. Ganesh, I.I. Misnon, R. Jose, Solvothermal synthesis of green fluorescent carbon dots from palm kernel shells, Proceedings, Materials Today, 2023.
[25] Y. Ji, X. Yang, Z. Ji, L. Zhu, N. Ma, D. Chen, X. Jia, J. Tang, Y. Cao, DFT-Calculated IR Spectrum Amide I, II, and III Band Contributions of N-Methylacetamide Fine Components, ACS, Omega 5 (2020) 8572–8578.
[26] F.S. Parker, Porphyrins and Related Compounds, in: F.S. Parker (Ed.), Applications of Infrared Spectroscopy in Biochemistry, Biology, and Medicine, Springer, US, Boston, MA, 1971, pp. 350–363.
[27] G.M. Alshammari, M.S. Al-Ayed, M.A. Abdelhalim, L.N. Al-Harbi, A.A. Qasem, M. A. Yahya, Development of luminescence carbon quantum dots for metal ions detection and photocatalytic degradation of organic dyes from aqueous media, Environ. Res. 226 (2023), 115661.
[28] Q. Li, T. Qin, Z. Bi, H. Hong, L. Ding, J. Chen, W. Wu, X. Lin, W. Fu, F. Zheng, Rac1 activates non-oxidative pentose phosphate pathway to induce chemoresistance of breast cancer, Nat. Commun. 11 (2020) 1456.
[29] R. Atchudan, T.N.J.I. Edison, K.R. Aseer, S. Perumal, N. Karthik, Y.R. Lee, Highly fluorescent nitrogen-doped carbon dots derived from Phyllanthus acidus utilized as a fluorescent probe for label-free selective detection of Fe3+ ions, live cell imaging and fluorescent ink, Biosens. Bioelectron. 99 (2018) 303–311.
[30] K. Jiang, X. Feng, X. Gao, Y. Wang, C. Cai, Z. Li, H. Lin, Preparation of multicolor photoluminescent carbon dots by tuning surface states, Nanomaterials 9 (2019) 529.
[31] N. Gao, W. Yang, H. Nie, Y. Gong, J. Jing, L. Gao, X. Zhang, Turn-on theranostic fluorescent nanoprobe by electrostatic self-assembly of carbon dots with doxorubicin for targeted cancer cell imaging, in vivo hyaluronidase analysis, and targeted drug delivery, Biosens. Bioelectron. 96 (2017) 300–307.
[32] W.-J. Long, X.-Q. Li, Y. Yu, C. He, Green synthesis of biomass-derived carbon dots as an efficient corrosion inhibitor, J. Mol. Liq. 360 (2022), 119522.
[33] H. Li, Z. Kang, Y. Liu, S.-T. Lee, Carbon nanodots: synthesis, properties and applications, J. Mater. Chem. 22 (2012) 24230–24253.
[34] T.-F. Yeh, W.-L. Huang, C.-J. Chung, I.-T. Chiang, L.-C. Chen, H.-Y. Chang, W.-C. Su, C. Cheng, S.-J. Chen, H. Teng, Elucidating quantum confinement in graphene oxide dots based on excitation-wavelength-independent photoluminescence, The Journal of Physical Chemistry Letters 7 (2016) 2087–2092.
[35] Y. Wang, A. Hu, Carbon quantum dots: synthesis, properties and applications, J. Mater. Chem. C 2 (2014) 6921–6939.
[36] M.K.A. Kolaprath, L. Benny, A. Varghese, A facile, green synthesis of carbon quantum dots from Polyalthia longifolia and its application for the selective detection of cadmium, Dyes Pigm. 210 (2023), 111048.
[37] J. Zong, Y. Zhu, X. Yang, J. Shen, C. Li, Synthesis of photoluminescent carbogenic dots using mesoporous silica spheres as nanoreactors, Chem. Commun. 47 (2011) 764–766.
[38] C. Zhao, Y. Jiao, L. Zhang, Y. Yang, One-step synthesis of S, B co-doped carbon dots and their application for selective and sensitive fluorescence detection of diethylstilbestrol, New J. Chem. 42 (2018) 2857–2864.
[39] S. Sarkar, D. Banerjee, U.K. Ghorai, N.S. Das, K.K. Chattopadhyay, Size dependent photoluminescence property of hydrothermally synthesized crystalline carbon quantum dots, J. Lumin. 178 (2016) 314–323.
[40] F. Wang, X.-K. Liu, S. Lai, J. Fang, D. Semin, Chromatographic studies of unusual on-column degradations of aniline compounds on XBridge Shield RP18 column in high pH aqueous mobile phase, J. Chromatogr. A 1218 (2011) 3502–3510.
[41] Z. Yan, T. Chen, L. Yan, X. Liu, J. Zheng, F.-D. Ren, Y. Yang, B. Liu, X. Liu, B. Xu, One-Step Synthesis of White-Light-Emitting Carbon Dots for White LEDs with a High Color Rendering Index of 97, Adv. Sci. 10 (2023) 2206386.
[42] P. Wu, W. Li, Q. Wu, Y. Liu, S. Liu, Hydrothermal synthesis of nitrogen-doped carbon quantum dots from microcrystalline cellulose for the detection of Fe3+ ions in an acidic environment, RSC Adv. 7 (2017) 44144–44153.
[43] W.-K. Li, J.-T. Feng, Z.-Q. Ma, Nitrogen, sulfur, boron and flavonoid moiety co-incorporated carbon dots for sensitive fluorescence detection of pesticides, Carbon 161 (2020) 685–693.
[44] Z. Deng, C. Liu, Y. Jin, J. Pu, B. Wang, J. Chen, High quantum yield blue-and orange-emitting carbon dots: one-step microwave synthesis and applications as fluorescent films and in fingerprint and cellular imaging, Analyst 144 (2019) 4569–4574.
[45] M. Pirsaheb, A. Asadi, M. Sillanpää, N. Farhadian, Application of carbon quantum dots to increase the activity of conventional photocatalysts: A systematic review, J. Mol. Liq. 271 (2018) 857–871.
[46] M. Najjar, M.A. Nasseri, A. Allahresani, M. Darroudi, Green and efficient synthesis of carbon quantum dots from Cordia myxa L. and their application in photocatalytic degradation of organic dyes, J. Mol. Struct. 1266 (2022), 133456.
[47] C. Thara, B. Mathew, Microwave synthesized N-doped carbon dots for dual mode detection of Hg (II) ion and degradation of malachite green dye, Talanta 125278 (2023).
[48] J. Ke, X. Li, Q. Zhao, B. Liu, S. Liu, S. Wang, Upconversion carbon quantum dots as visible light responsive component for efficient enhancement of photocatalytic performance, J. Colloid Interface Sci. 496 (2017) 425–433.
[49] A. Zuorro, R. Lavecchia, M.M. Monaco, G. Iervolino, V. Vaiano, Photocatalytic degradation of azo dye reactive violet 5 on Fe-doped titania catalysts under visible light irradiation, Catalysts 9 (2019) 645.
[50] A. Ajmal, I. Majeed, R.N. Malik, H. Idriss, M.A. Nadeem, Principles and mechanisms of photocatalytic dye degradation on TiO 2 based photocatalysts: a comparative overview, RSC Adv. 4 (2014) 37003–37026.
[51] M.A. Fox, M.T. Dulay, Heterogeneous photocatalysis, Chem. Rev. 93 (1993) 341–357.
[52] S. Chaudhary, S. Goyal, A. Umar, Fabrication of biogenic carbon-based materials from coconut husk for the eradication of dye, Chemosphere 340 (2023), 139823.